International Journal of Nanomedicine

Dovepress
open access to scientific and medical research

Open Access Full Text Article

ORIGINAL RESEARCH

Vancomycin-modified Fe_3O_4@SiO_2@Ag microflowers as effective antimicrobial agents

This article was published in the following Dove Press journal:
International Journal of Nanomedicine
13 April 2017
Number of times this article has been viewed

Chongwen Wang[1,2,*]
Kehan Zhang[2,*]
Zhe Zhou[2,*]
Qingjun Li[2]
Liting Shao[2]
Rong Zhang Hao[3]
Rui Xiao[2]
Shengqi Wang[1,2]

[1]College of Life Sciences & Bio-Engineering, Beijing University of Technology, [2]Beijing Key Laboratory of New Molecular Diagnosis Technologies for Infectious Diseases, Beijing Institute of Radiation Medicine, Beijing, [3]Institute for Disease Control and Prevention, Academy of Military Medical Sciences, Beijing, People's Republic of China

*These authors contributed equally to this work

Abstract: Nanomaterials combined with antibiotics exhibit synergistic effects and have gained increasing interest as promising antimicrobial agents. In this study, vancomycin-modified magnetic-based silver microflowers (Van/Fe_3O_4@SiO_2@Ag microflowers) were rationally designed and prepared to achieve strong bactericidal ability, a wide antimicrobial spectrum, and good recyclability. High-performance Fe_3O_4@SiO_2@Ag microflowers served as a multifunction-supporting matrix and exhibited sufficient magnetic response property due to their 200 nm Fe_3O_4 core. The microflowers also possessed a highly branched flower-like Ag shell that provided a large surface area for effective Ag ion release and bacterial contact. The modified-vancomycin layer was effectively bound to the cell wall of bacteria to increase the permeability of the cell membrane and facilitate the entry of the Ag ions into the bacterium, resulting in cell death. As such, the fabricated Van/Fe_3O_4@SiO_2@Ag microflowers were predicted to be an effective and environment-friendly antibacterial agent. This hypothesis was verified through sterilization of Gram-negative *Escherichia coli* and Gram-positive methicillin-resistant *Staphylococcus aureus*, with minimum inhibitory concentrations of 10 and 20 μg mL^{-1}, respectively. The microflowers also showed enhanced effect compared with bare Fe_3O_4@SiO_2@Ag microflowers and free-form vancomycin, confirming the synergistic effects of the combination of the two components. Moreover, the antimicrobial effect was maintained at more than 90% after five cycling assays, indicating the high stability of the product. These findings reveal that Van/Fe_3O_4@SiO_2@Ag microflowers exhibit promising applications in the antibacterial fields.

Keywords: antibiotic-resistant bacteria, surface area, biological properties, magnetic composites, Ag shell

Introduction

The increasing risk of antibiotic-resistant bacterial infections is a serious problem to health care; this condition decreases the efficiency of conventional antibiotics and significantly increases the number of clinical infections.[1,2] In this regard, scholars have focused on developing new generations of effective antibacterial agents, such as antibacterial nanomaterials, to meet the urgent need of reducing antibiotic abuse.[3] The use of nanomaterials, which exhibit high specific surface area and unique physical, chemical, and biological properties, offers new approaches for rapid and effective killing of pathogenic microorganisms.[4] In contrast to the mechanistic action of antibiotics, nanomaterials target multiple bacterial components; as such, microbes cannot easily acquire resistance toward these particles.[5] Many nanomaterials, including gold,[6] silver,[7] copper,[8] zinc oxide,[9] and graphene oxide,[10] exhibit excellent bactericidal activity; of these, Ag nanomaterials possess the optimal antibacterial activity because they kill most pathogenic microbes, including bacteria, fungi, and viruses.[11,12] Thus far, no organism has readily developed resistance to Ag nanomaterials.[13] Moreover,

Correspondence: Rui Xiao; Shengqi Wang
Beijing Key Laboratory of New Molecular Diagnosis Technologies for Infectious Diseases, Beijing Institute of Radiation Medicine, Taiping Road 27, Haidian District, Beijing 100850, People's Republic of China
Email zhouzhe@bmi.ac.cn; ruixiao203@sina.com

submit your manuscript | www.dovepress.com
Dovepress
http://dx.doi.org/10.2147/IJN.S132570

Ag nanomaterials feature low toxicity to human body and are widely applied in water purification systems, wound dressings, surgery instruments, and implantable materials.[14] Thus, various Ag-based nanoparticles have been extensively studied as potent and broad-spectrum antimicrobial agents.

However, the practical application of these Ag-based nanomaterials is hindered by three limitations that should be addressed urgently. First, the irregular aggregation of small Ag nanoparticles (Ag NPs) reduces or diminishes typical properties associated with their nanoscale size.[15] Ag NPs elicit antibacterial activity due to their nanometer size; that is, small particles exhibit increased activities based on the equivalent Ag mass content.[16] Nevertheless, Ag NPs with a diameter less than 20 nm tend to aggregate, thereby reducing their antibacterial activity.[17] The second issue is the recovery of disinfectants in water environment. The Ag NPs are very small, which makes it difficult to eliminate them completely by centrifugation or filtration, and high concentrations of residual nanosilver in solution can cause potential adverse health effects.[18] Third, Ag-based nanomaterials exhibit inferior activity against Gram-positive bacterial pathogens compared with that against Gram-negative bacteria; this phenomenon could be attributed to the thicker and more stable membrane of the former than that of the latter. This feature prevents the Ag ions from entering into the bacterium.[19,20] However, bacterial infections caused by Gram-positive pathogens are the leading causes of morbidity and mortality in humans.[21] To overcome these drawbacks, researchers must investigate the combination of Ag NPs with other materials in the field of sterilization.

Recyclability can be achieved using magnetic materials to load Ag NPs, allowing the particles to be easily separated from water solution by magnetic forces.[22] Magnetic particles serve as a proper supporting platform for immobilizing Ag particles to form homogeneous ultrafine Ag nanostructures without aggregation.[23] The large surface area of the magnetic nanocomposites allows high loading and sufficient contact area to achieve high antibacterial efficacy. As such, Ag-loaded magnetic particles have been increasingly applied in antibacterial research. Many kinds of Ag-based magnetic composites have been successfully synthesized.[17,24–26] However, the antibacterial effect of the fabricated magnetic composites on Gram-positive bacteria remains insufficient.

On the other hand, a number of researchers reported the synergistic antibacterial effects of metal NPs with conventional antibiotics.[27–30] For example, Brown et al indicated the effective synergistic effect of noble metal NPs functionalized with ampicillin against multiresistant strains.[31] Lai et al reported a general route for preparing vancomycin-modified Au NPs; the products act as effective broad-spectrum bactericides against both Gram-negative and Gram-positive pathogens.[32] These studies have focused on synthesis of different antibiotic-functional nanostructures and investigated their enhanced antibacterial activity. However, the combination of Ag-based magnetic composites and antibiotics as effective antibacterial agents has been rarely reported yet.

In the present study, we propose the use of a novel vancomycin-modified Fe_3O_4@SiO_2@Ag microflower for rapid and effective killing of pathogenic bacteria in solutions. The hybrid microcomposite combines the unique properties of the magnetic core, flower-like Ag shell, and modified-vancomycin layer. The microcomposite shows significantly enhanced antibacterial activity and is environment friendly. High-performance Fe_3O_4@SiO_2@Ag microflowers with good dispersity, uniform structure, and sufficient magnetic responsiveness were prepared via our proposed sonochemical-based method and used as the core component.[33] Compared with the conventional smooth Ag shell, the highly branched flower-like Ag shell provided larger surface area for effective Ag ion release and bacterial contact. Vancomycin was selected for binding to the Fe_3O_4@SiO_2@Ag microflowers to maximize the bactericidal potential; this antibiotic exhibits a well-established mechanism and synergistic antibacterial effects with various types of NPs.[34,35] Vancomycin can directly bind to the terminal D-Ala-D-Ala portion of the peptidoglycan of the cell wall of a Gram-positive bacterium through hydrogen bonds to inhibit peptidoglycan synthesis. Moreover, previous studies have demonstrated that vancomycin-modified NPs elicit enhanced antimicrobial activities or can electively capture not only Gram-positive but also Gram-negative bacterium.[36,37] The fabricated Van/Fe_3O_4@SiO_2@Ag microflowers were subjected to antibacterial tests against both Gram-positive and Gram-negative bacteria, and we concluded that a combination of vancomycin and Fe_3O_4@SiO_2@Ag microflowers as antibacterial agents could lead to better antimicrobial activity through their synergistic effects. To the best of our knowledge, this study is the first to investigate the synergistic effect of magnetic-based Ag microcomposites and vancomycin for sterilization. Additionally, the recyclability of Van/Fe_3O_4@SiO_2@Ag microflowers was evaluated over five washing-and-reuse cycles to determine their potential in practical applications.

Experimental methods

Materials and chemicals

Tetraethoxysilane (TEOS), *n*-butylamine, silver nitrate, vancomycin, polyvinylpyrrolidone (PVP, 40 kDa), *N*-(3-dimethylaminopropyl)-*N*′-ethylcarbodiimide hydrochloride

(EDC), 11-mercaptoundecanoic acid (MUA), and 2-(*N*-morpholino)ethanesulfonic acid (MES) were obtained from Sigma-Aldrich Chemicals Co. (St Louis, MO, USA). Ferric chloride ($FeCl_3 \cdot 6H_2O$), ethylene glycol (EG), diethylene glycol (DEG), trisodium citrate, sodium acetate anhydrous (NaOAc), and phosphate-buffered saline (PBS) buffer (10 mM, pH 7.4) were purchased from Sinopharm Chemical Reagent Co., Ltd. (Shanghai, People's Republic of China). All chemicals were of analytical grade and were utilized as received unless mentioned otherwise. All aqueous solutions were purified with a Milli-Q system (18.2 MΩ cm^{-1}). Commercial *Escherichia coli* (BL21) and clinical isolation strains of methicillin-resistant *Staphylococcus aureus* (MRSA) were provided by the Institute for Disease Control and Prevention, Academy of Military Medical Sciences.

Synthesis of Fe_3O_4 and Fe_3O_4@SiO_2 microspheres

Superparamagnetic Fe_3O_4 particles (~200 nm) were synthesized by modified solvothermal reaction.[38] In a typical procedure, 1 g of $FeCl_3 \cdot 6H_2O$ (≈4 mmol) was dissolved in a mixture of DEG and EG (V_{DEG}/V_{EG} =13/7; total volume of 40 mL) in an explosion-proof bottle under magnetic stirring. The solution was added with 4 g of PVP and heated at 120°C for 30 min until a transparent solution was obtained. Then, the solution was added with 3 g of NaOAc, and heating was terminated. After stirring for an additional hour, the obtained homogeneous solution was sealed in a Teflon-lined stainless steel autoclave (100 mL volume) and then transferred to a vacuum oven, which was preheated to 200°C. After a 10-h reaction period, the solution was cooled to room temperature, and the obtained Fe_3O_4 particles were collected with an external magnet, washed five times with ethanol and water, and then dried in vacuum at 60°C for 6 h.

The synthesis of Fe_3O_4@SiO_2 microspheres was carried out according to a modified Stöber method. Briefly, 0.1 g of as-prepared Fe_3O_4 microspheres was dispersed in a mixture of ethanol–water–ammonia (180 mL/10 mL/8 mL) by sonication for 15 min. Subsequently, 0.3 mL of TEOS solution was consecutively added to the mixture under vigorous sonication for 1 h. The resulting Fe_3O_4@SiO_2 microspheres were magnetically separated and washed and then redispersed in 10 mL of anhydrous ethanol.

Synthesis of Fe_3O_4@SiO_2–Ag seed microspheres

To synthesize Fe_3O_4@SiO_2–Ag seed microspheres, 0.1 g of Fe_3O_4@SiO_2 microspheres was thoroughly washed with anhydrous ethanol and then dispersed in 1 mL of anhydrous ethanol by ultrasonic irradiation. In a typical deposition procedure, the cleaned Fe_3O_4@SiO_2 microspheres were mixed with 9 mL of the silver nitrate solution (0.8 mM) and incubated at 30°C for 30 min under sonication. Then, the reaction tube was then added with 80 µL of butylamine (100 mM). The mixture was ultrasonically irradiated for 1 h to allow the deposition of small and dense Ag seeds onto the Fe_3O_4@SiO_2 surface. Finally, the products were magnetically separated from the suspension and redispersed in ethanol, and the solution was called Fe_3O_4@SiO_2–Ag seed solution.

Synthesis of Fe_3O_4@SiO_2@Ag microflowers

Briefly, 1 mL of the prepared Fe_3O_4@SiO_2–Ag seed was added into 400 mL of the $AgNO_3$ aqueous solution (0.2 mM) to obtain high-performance Fe_3O_4@SiO_2@Ag microflowers. The mixture was added with 400 µL of 37% formaldehyde and 800 µL of 25% ammonia solution successively. After a 5-min reaction period, the solution was added with 600 mg of PVP powder and sonicated for another 15 min. Finally, the products were collected and rinsed several times with deionized water to remove excess PVP.

Immobilization of vancomycin onto the surface of Fe_3O_4@SiO_2@Ag microflowers

For the preparation of vancomycin-modified Fe_3O_4@SiO_2@Ag microflowers, the microflowers were carboxyl-group-functionalized first and then conjugated with vancomycin according to a previously reported method.[36] In brief, Fe_3O_4@SiO_2@Ag microflowers (10 mg/mL) were incubated overnight in an MUA ethanol solution (20 µM) to obtain surface-carboxylated microflowers. Then, the prepared MUA/Fe_3O_4@SiO_2@Ag microflowers in 10 mL of MES buffer (0.1 M, pH 5) were mixed with 1 mL of EDC (10 mg/mL) and sonicated for 5 min. The mixture was then added with 1 mL of vancomycin (5 mg/mL) and sonicated for 2 h. The resulting Van/Fe_3O_4@SiO_2@Ag microflowers were washed with water and redispersed in PBS buffer (10 mM, pH 7.4).

Material characterization

Scanning electron microscopy (SEM) images were taken on a JEOL JSM-7001F microscope operating at 10 kV. Transmission electron microscopy (TEM) images were taken with a Hitachi H-7650 microscope operating at 80 kV. High-resolution TEM (HRTEM) images and energy-dispersive X-ray spectroscopy (EDX) spectra were obtained using a JEOL JEM-2010F microscope at an accelerating

voltage of 200 kV. UV–vis spectra were obtained using a Shimadzu 2600 spectrometer. Magnetic characterization was conducted with a superconducting quantum interference device magnetometer (SQUID, MPMSXL-7) at 300 K. The X-ray diffraction (XRD) patterns of the products were investigated by a Japan Rigaku D/max 2550 VB/PC rotation anode X-ray diffractometer. Zeta potential of products was measured by dynamic light scattering with Zetasizer Nano ZS (NANO-ZS 90; Malvern Instruments, Malvern, UK). A simultaneous differential scanning calorimetry/thermogravimetric analysis (DSC/TGA) was performed to characterize the decomposition and thermal stability of products measured from 30°C to 600°C at the heating rate of 10°C/min.

Antibacterial tests

For the antibacterial activity tests, two bacterial species, Gram-negative *E. coli* BL21 and Gram-positive MRSA, were used in the experiments. *E. coli* BL21 was cultured in Luria–Bertani medium, and MRSA was cultured in trypticase soy broth medium. After 8 h, the concentration of the bacteria was determined by the optical density (OD) at 600 nm based on the turbidity of the cell suspension.[39] Subsequently, the bacterial suspension was diluted by PBS buffer (10 mM, pH 7.4), and a final density of 10^4 cells/mL was obtained for the antibacterial tests. One hundred microliters of the bacterial suspension was inoculated in 10 mL of the culture medium supplemented with different amounts of Van/Fe_3O_4@SiO_2@Ag microflowers. The suspensions were shaken at 200 rpm at 37°C for 10 h, and then the bacterial survival was withdrawn and determined by measuring the absorbance at 600 nm. The control group was prepared under the similar condition in the absence of Van/Fe_3O_4@SiO_2@Ag microflowers and the presence of Fe_3O_4@SiO_2@Ag microflowers for comparison. Classical culture method was performed to study the antibacterial activity of Fe_3O_4@SiO_2@Ag microflowers and vancomycin-modified microflowers. One hundred microliters of the above-treated bacterial suspension was diluted by 10^5 times serially by PBS buffer and directly cultured on an agar plate and incubated at 37°C. After 24 h, the number of colonies was counted to evaluate the survival condition of the bacterial cells.

Results and discussion

Fabrication of vancomycin-modified Fe_3O_4@SiO_2@Ag microflowers

As illustrated in Scheme 1A, vancomycin-modified Fe_3O_4@SiO_2@Ag microflowers were fabricated in five steps. Superparamagnetic Fe_3O_4 particles (~200 nm) used as the magnetic core were synthesized through a modified solvothermal reaction at 200°C. Then, Fe_3O_4@SiO_2

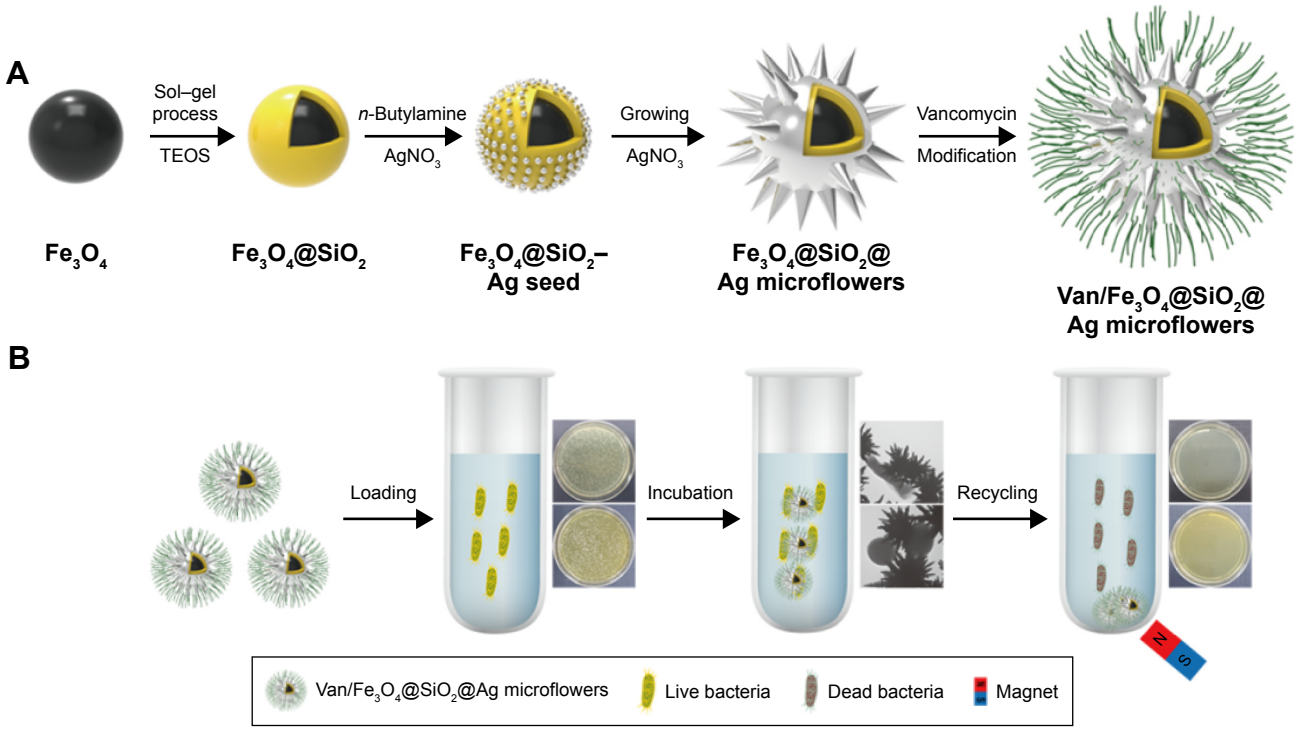

Scheme 1 (**A**) Synthesis route of Van/Fe_3O_4@SiO_2@Ag microflowers. (**B**) Schematic of the operating procedures for bacterial killing in solution by Van/Fe_3O_4@SiO_2@Ag microflowers.
Abbreviation: TEOS, tetraethoxysilane.

microspheres were prepared by coating the Fe_3O_4 core with a thicker silica shell (~50 nm) via a fast sol–gel method using sonication. The silica shell of magnetic structure efficiently dispersed the particles in the aqueous solution and provided functional groups for deposition of the Ag seeds. We employed a butylamine reduction system to deposit dense Ag seeds onto the surface of the Fe_3O_4@SiO_2 particles. Subsequently, the Fe_3O_4@SiO_2@Ag microflowers were synthesized through ultrasound-assisted seed-mediated growth strategy according to our previous publication.[33] All Ag seeds isotropically grew within a few seconds and were stabilized by PVP. Finally, vancomycin-coated microflowers were synthesized via a two-step coupling method: 1) Fe_3O_4@SiO_2@Ag microflowers were carboxyl-group-functionalized through MUA modification and 2) the vancomycin was modified on the surface of the carboxylated Fe_3O_4@SiO_2@Ag microflowers through carbodiimide chemistry.

Characterization of Fe_3O_4@SiO_2@Ag microflowers

TEM and SEM analyses were applied to characterize the morphology of the as-obtained products during different stages. Figure 1A shows the typical TEM image of the monodispersed Fe_3O_4 particles with a diameter of ~200 nm. The uniform Fe_3O_4 spherical particles were synthesized by the modified solvothermal method, where PVP was used to improve the water dispersibility. The silica coating was created by the simple sol–gel process. The silica shell thickness could be easy controlled by varying the concentration of TEOS.[40] Figure 1B presents the TEM image of uniform Fe_3O_4@SiO_2 microspheres with an obvious core/shell structure. The silica shell is clearly visible and possesses ~50 nm thickness. The zeta potential of Fe_3O_4@SiO_2 in ethanol was −31.3 mV, indicating that the surface hydroxyl groups of silica shell were deprotonated in absolute ethanol (Figure S1). The negatively charged Fe_3O_4@SiO_2 particles adsorbed Ag^+ ions as nucleation centers for further Ag seed formation. After the Ag^+ ions were bound to the SiO_2 shell sufficiently, $AgNO_3$ was reduced by butylamine and conjugated to the silica surface. Figure 1C shows that the dense and relatively uniform Ag seeds successfully coated the Fe_3O_4@SiO_2 particles. The size of the deposited seeds was ~10–20 nm. The deposition of the Ag seeds was also confirmed based on the SEM image (Figure 1E), which shows that these particles are well distributed on the Fe_3O_4@SiO_2 microspheres. Butylamine is a mild reductant; as such, excess nucleation centers were not formed in the solution.[41] The particle size and density of the Ag seeds on the SiO_2 surface can be controlled by tuning the concentrations of butylamine and $AgNO_3$.[42] Figure S2 shows the Fe_3O_4@SiO_2–Ag seed particles synthesized with

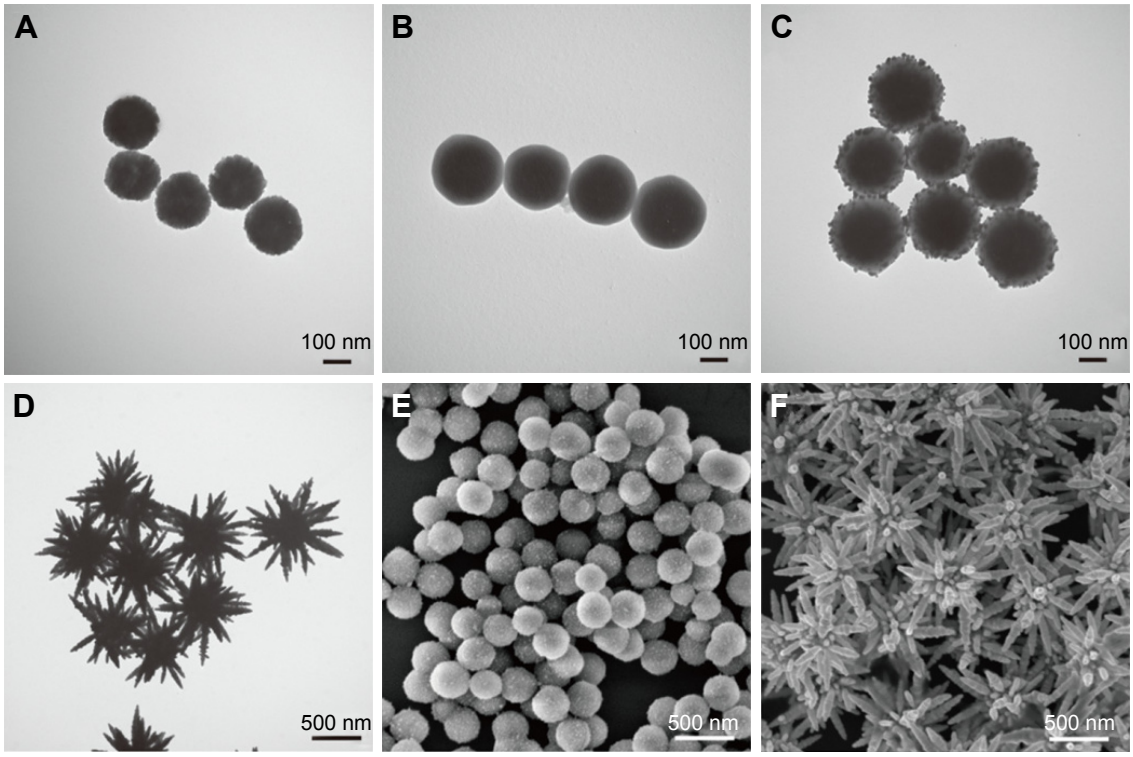

Figure 1 (*Continued*)

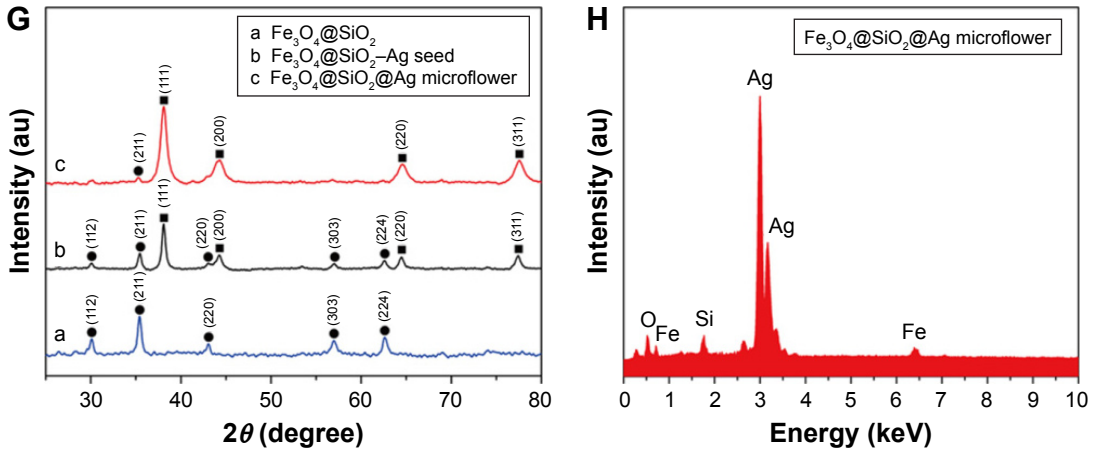

Figure 1 Characterization of Fe_3O_4@SiO_2@Ag microflowers. Transmission electron microscopy images of (**A**) Fe_3O_4, (**B**) Fe_3O_4@SiO_2, (**C**) Fe_3O_4@SiO_2–Ag seed, and (**D**) Fe_3O_4@SiO_2@Ag microflowers. Scanning electron microscopy images of (**E**) Fe_3O_4@SiO_2–Ag seed and (**F**) Fe_3O_4@SiO_2@Ag microflowers. (**G**) X-ray diffraction patterns and (**H**) energy-dispersive X-ray spectra of Fe_3O_4@SiO_2@Ag microflowers. The circles represent the peaks of the magnetite structure of Fe_3O_4. The squares indicate the peaks of cubic Ag.

different conditions. The TEM images of all the seed particles were obtained after the deposition of the Ag particles in a mixture of $AgNO_3$ and butylamine at a molar ratio of 1:1. When 0.2, 0.4, and 0.8 mM $AgNO_3$ and butylamine were added to the Fe_3O_4@SiO_2 ethanol solution, abundant and small Ag seeds were deposited uniformly on the SiO_2 surface. Fe_3O_4@SiO_2–Ag seed synthesized with 0.8 mM $AgNO_3$ and butylamine was found to be the optimal seed particle for flower-like Ag petal growth. Seed-mediated growth was determined as the mechanism underlying the formation of the flower-like Ag shell produced by a one-step redox reaction in the presence of suitable Ag seeds deposited on the Fe_3O_4@SiO_2 microspheres. The flower-like shell formation was rapidly completed by ultrasound-driven synthesis, where the Ag seeds acted as nucleation sites for rapid anisotropy. Superfluous $AgNO_3$ is necessary in the reaction system because a high reactant concentration promotes the formation of highly branched structures. The fast-growing Ag petals consumed large amounts of Ag atoms. When ammonia was injected, Ag^+ ions were reduced by CH_2O immediately and quickly deposited on the Ag seeds of silica surface, resulting in the formation of flower-like Ag shells surrounding the magnetic cores. Figure 1D shows the TEM picture of the obtained Fe_3O_4@SiO_2@Ag microflowers, which possess a highly branched morphology and are nearly uniform with a particle diameter ranging from 700 to 900 nm. The SEM image in Figure 1F shows that the microflowers are composed of numerous flower-like Ag petals and ultrasharp Ag tips. All the magnetic-based Ag microflowers exhibit relatively uniform morphology and size. Furthermore, the TEM and SEM images indicate the successful controllable synthesis of high-performance Fe_3O_4@SiO_2@Ag microflowers. PVP was used as a stabilizer to limit particle aggregation. In sample without PVP, Fe_3O_4@SiO_2@Ag microflowers were formed but would be easily aggregated (Figure S3A); this aggregation process is irreversible. When the concentration of PVP reached 1 mg/mL, the dispersibility of the microflower particles improved (Figure S3B).

The as-prepared samples were also examined by XRD analysis (Figure 1G). Curve a in Figure 1G shows the XRD spectra of the Fe_3O_4@SiO_2 microspheres, which fitted well to the Fe_3O_4 bulk phases (JCPDS card no 75-1609).[43,44] As the SiO_2 shell was amorphous, no diffraction peaks corresponding to SiO_2 were observed. With the deposition of Ag seeds, four additional diffraction peaks were observed at 2θ values of 38.2°, 44.3°, 64.5°, and 77.5°, which correspond to the reflections of the (111), (200), (220), and (311) crystal planes of Ag, respectively (curve b of Figure 1G). These peaks correspond to the cubic-phase Ag (JCPDS no 04-0783) and indicate that dense Ag seeds were successfully deposited on the surface of Fe_3O_4@SiO_2 microspheres.[45,46] The XRD pattern of the Fe_3O_4@SiO_2@Ag microflowers showed an obvious increase in the intensity of the Ag peaks when the highly branched Ag shell was formed outside the magnetic core (curve c of Figure 1G). The EDX spectrum (Figure 1H) of the Fe_3O_4@SiO_2@Ag microflower confirms that the microflower particles mainly consist of Fe, Si, O, and Ag. No other impurity peaks were detected in the EDX spectrum, indicating the purity of the final product.

The UV–vis absorbance of the as-obtained products is shown in Figure 2A. Curves a and b denote the typical UV–vis spectra of Fe_3O_4 and Fe_3O_4@SiO_2 microspheres, respectively. After the small Ag seeds were deposited, a broad absorption peak appeared at ~450 nm due to the Mie plasmonic

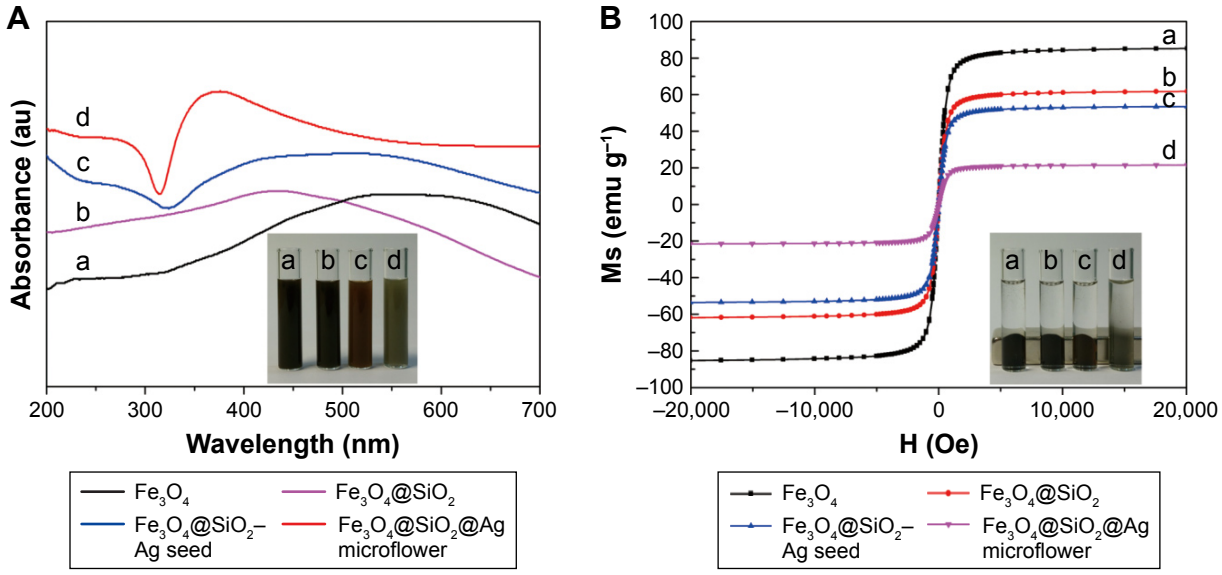

Figure 2 (**A**) UV–vis spectra and (**B**) magnetic hysteresis curves of the prepared Fe_3O_4, Fe_3O_4@SiO_2, Fe_3O_4@SiO_2–Ag seed microspheres, and Fe_3O_4@SiO_2@Ag microflowers. Insets in (**A**) and (**B**) show suspensions before and after magnetic enrichment by an external magnetic force, respectively.

resonance from the neighboring silver particles (curve c of Figure 2A).[47] After the flower-like shell was formed outside the magnetic core, the obvious absorption peak became strong and blue-shifted to ~375 nm (curve d of Figure 2A). This phenomenon can be ascribed to the strong plasmon coupling between neighboring Ag petals. Hence, the highly branched Ag shell coated the magnetic core.

The magnetic properties of as-prepared samples were investigated with a SQUID magnetometer. The saturation magnetization (MS) values of Fe_3O_4, Fe_3O_4@SiO_2, Fe_3O_4@SiO_2–Ag seed, and Fe_3O_4@SiO_2@Ag microflowers were 85.2, 61.7, 53.5, and 21.4 emu g^{-1}, respectively (Figure 2B). The MS values gradually decreased after SiO_2 coating, Ag seed deposition, and flower-like Ag shell formation. This result can be explained by the increasing number of nonmagnetic coating materials formed around the Fe_3O_4 cores. Despite the significant decrease in the MS value of the Fe_3O_4@SiO_2@Ag microflowers, the magnetization of the final structure remained sufficient for fast magnetic separation. All of the curves nearly intersected with the origin, indicating that the synthesized products were in a superparamagnetic state at room temperature. These excellent magnetic properties confer the microflowers with great potential in bioseparation and biodetection.

Characterization of vancomycin-modified Fe_3O_4@SiO_2@Ag microflowers

Figure 3A shows the modification method for depositing vancomycin molecules onto the surface of the fabricated Fe_3O_4@SiO_2@Ag microflowers. MUA was used to form a bifunctional linker, which not only provided terminal carboxyl group for subsequent coupling reaction but also acted as a suitable arm for reducing the steric hindrance between vancomycin and bacteria. MUA-modified Fe_3O_4@SiO_2@Ag microflowers were easily obtained by treating MUA under sonication with the formation of strong covalent Ag–S bond.[48] The carboxyl groups on the Fe_3O_4@SiO_2@Ag microflowers surface were bound with vancomycin via carbodiimide activation to yield vancomycin-modified Fe_3O_4@SiO_2@Ag microflowers. HRTEM analysis was performed to obtain detailed insights into the surface structure of the Van/Fe_3O_4@SiO_2@Ag microflowers (Figure 3B and C). The HRTEM picture obtained from the edge of flower-like Ag shells (Figure 3C) shows that the Fe_3O_4@SiO_2@Ag microflowers are surrounded by a thin membrane-like layer with ~1.5 nm thickness. This membrane-like structure was formed by MUA and vancomycin. To confirm that vancomycin was successfully modified on the Fe_3O_4@SiO_2@Ag microflowers, we used elemental mapping for analysis of the presence and spatial distribution of the N component. Figure 3D shows the bright-field TEM image of a part of an individual Fe_3O_4@SiO_2@Ag microflower. Figure 3E–I shows the elemental mapping of the sample, where Fe is located in the magnetic core, Si and Ag are distributed throughout the entire composite, and N is mainly located on the surface of the microflower. In the designed Van/microflower structure, N was only derived from the vancomycin molecules. Therefore, the intensive N signal confirms that Fe_3O_4@SiO_2@Ag microflower was successfully conjugated with vancomycin.

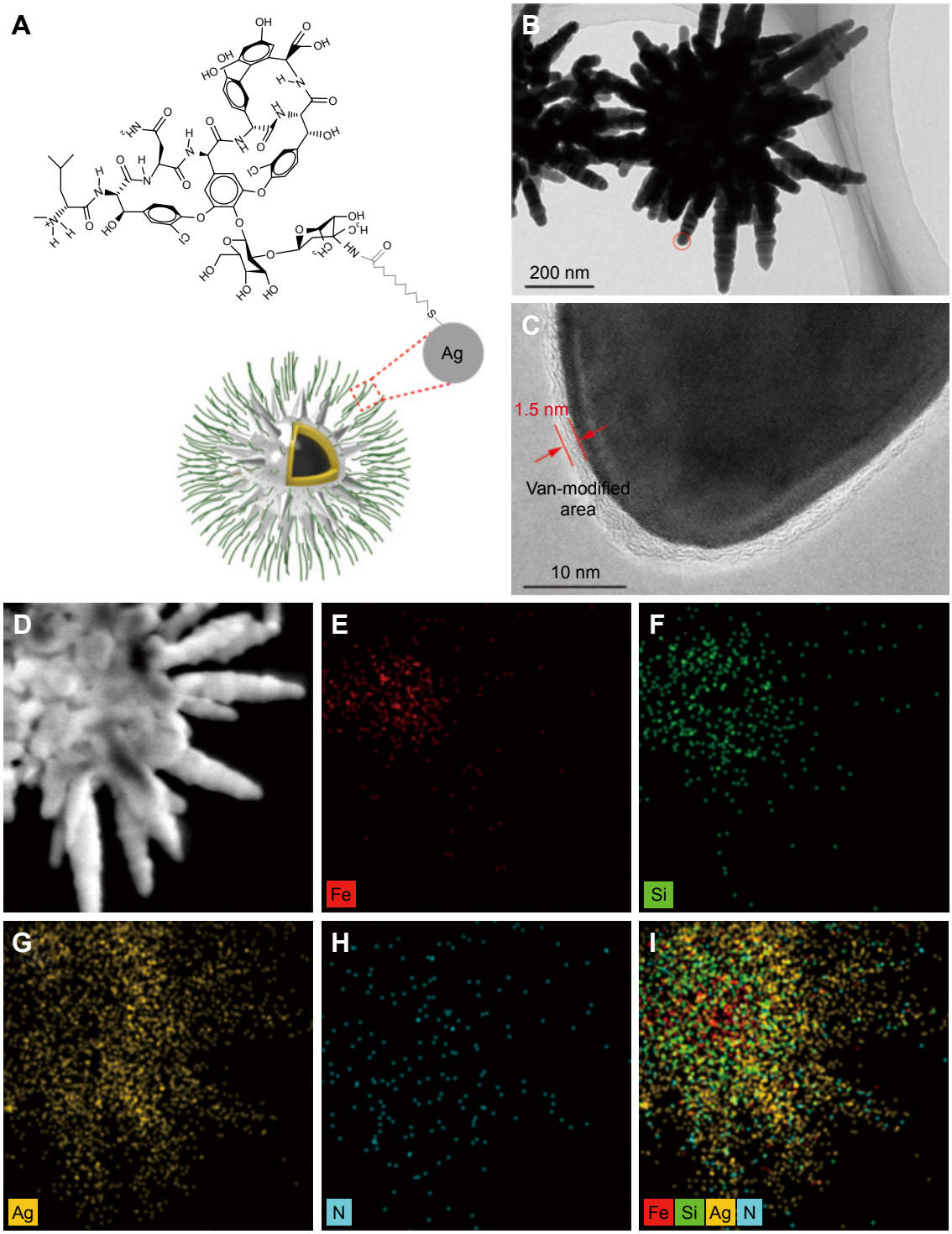

Figure 3 Characterization of Van/Fe_3O_4@SiO_2@Ag microflowers. (**A**) Schematic of the molecular structure of vancomycin and its coupling interaction with Fe_3O_4@SiO_2@Ag microflowers. (**B**) High-resolution transmission electron microscopy image of the vancomycin-modified Fe_3O_4@SiO_2@Ag microflower and (**C**) the corresponding magnified image obtained from the circled area in (**B**). Arrows indicate a thin membrane-like layer of vancomycin and 11-mercaptoundecanoic acid. (**D**) The bright-field transmission electron microscopy image of a part of an individual Fe_3O_4@SiO_2@Ag microflower. (**E–I**) The associated elemental mappings showing the element distributions of Fe (red), Si (green), Ag (yellow), and N (blue) in the composite.

The UV–vis absorption spectra of vancomycin solution before and after the conjugation reaction were also examined (Figure S4). The absorption intensity at 280 nm of the supernatant of the MUA/Fe_3O_4@SiO_2@Ag microflowers significantly decreased after vancomycin conjugation. This result further confirms that the vancomycin molecules were effectively bound to the Fe_3O_4@SiO_2@Ag microflowers surface. Moreover, a simple experiment was carried out to

investigate the bonding strength of vancomycin molecules to the Fe_3O_4@SiO_2@Ag microflowers. In this test, 0.1 g of the Van/Fe_3O_4@SiO_2@Ag microflowers was continuously stirred in 10 mL of distilled water at room temperature overnight. A filtered sample of the solution was obtained, and its UV–vis spectrum was recorded. Vancomycin showed an absorption band at ~280 nm in its UV–vis spectrum. However, the spectrum of the filtered solution did not show any absorption band in this range. This finding indicates the absence of vancomycin in the filtered solution, suggesting the strong coupling of vancomycin molecule to the Ag microflowers.

Antibacterial properties of vancomycin-modified Fe_3O_4@SiO_2@Ag microflowers

We evaluated the sterilizing effect of the synthesized Van/Fe_3O_4@SiO_2@Ag microflowers on *E. coli* and MRSA as model Gram-negative and Gram-positive bacteria, respectively, both of which represent the leading multidrug-resistant bacterial pathogens. Bacterial inhibition growth curves were plotted to investigate the antibacterial abilities of the Fe_3O_4@SiO_2@Ag microflowers alone and in combination with vancomycin. Diluted solutions of the products were incubated with 10 mL of bacterial suspension (about 10^4 CFU/mL), and the control group was subjected to a similar condition in the absence of synthesized microflowers for comparison. The results of bacterial proliferation were determined by the OD at 600 nm of the suspension. The concentration-induced antibacterial results are shown in Figure 4A and B.

The fabricated Van/Fe_3O_4@SiO_2@Ag microflowers slowed down the growth of both strains (*E. coli* and MRSA). Remarkably, the minimum inhibitory concentrations (MICs) of the vancomycin-modified Fe_3O_4@SiO_2@Ag microflowers were 10 μg mL^{-1} for *E. coli* and 20 μg mL^{-1} for MRSA. Moreover, the antibacterial ability of Van/Fe_3O_4@SiO_2@Ag microflowers was significantly higher than that of the non-modified microflowers. For both strains, Fe_3O_4@SiO_2@Ag microflowers at a concentration of 20 μg mL^{-1} did not restrain the bacterial growth after 5 h, whereas the Van/Fe_3O_4@SiO_2@Ag microflower-treated group showed almost 100% killing efficiency under the same experimental condition. The Fe_3O_4@SiO_2@Ag microflowers could be an efficient antibacterial agent because its flower-like Ag shell provides larger active surface areas for contacting bacteria and releasing Ag ions than those of conventional smooth Ag shell. Figure S5 shows the result of incubating the same bacterial sample with the Fe_3O_4@SiO_2@Ag microflower alone overnight. The MIC values of Fe_3O_4@SiO_2@Ag microflowers were 25 μg mL^{-1} for Gram-negative *E. coli* and 55 μg mL^{-1} for Gram-positive MRSA. We conclude that the MIC decreased by about 60% for *E. coli* and 63.5% for MRSA when using only Fe_3O_4@SiO_2@Ag microflowers.

Plate counting method was carried out to assess the antibacterial ability of the obtained microstructures in different stages.[49] Approximately 100 μL of the overnight-cultured bacterial suspension was diluted to 10^3 cells/mL with medium, and then spread onto the agar plates, and cultured at 37°C overnight. Figure 4C shows the formation

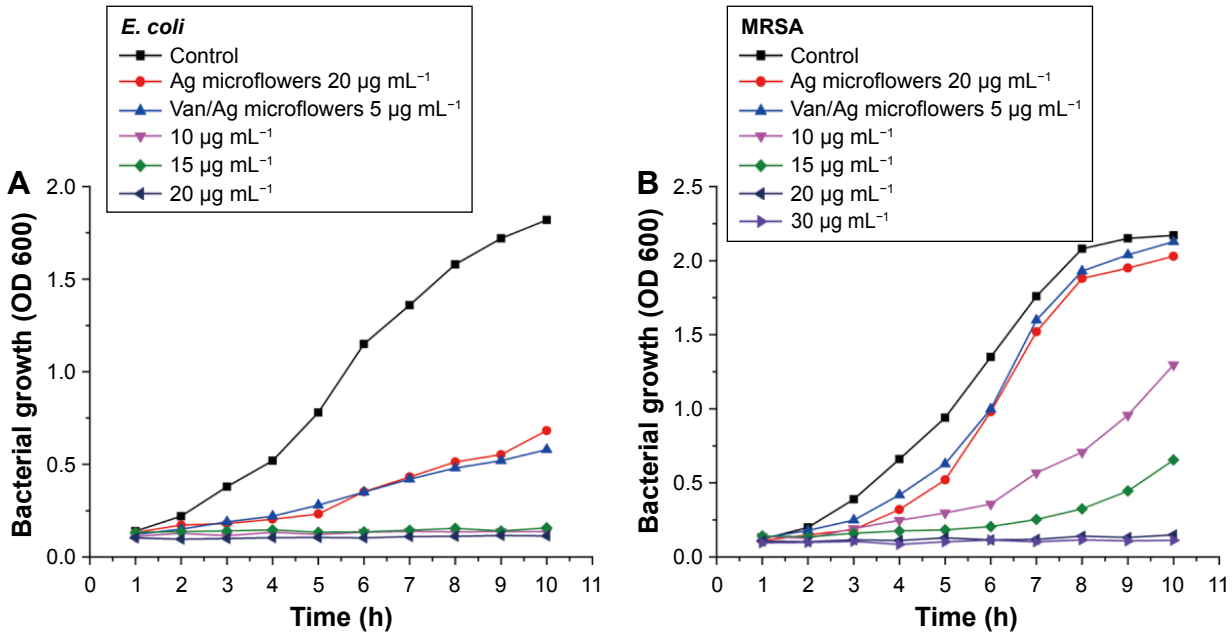

Figure 4 (*Continued*)

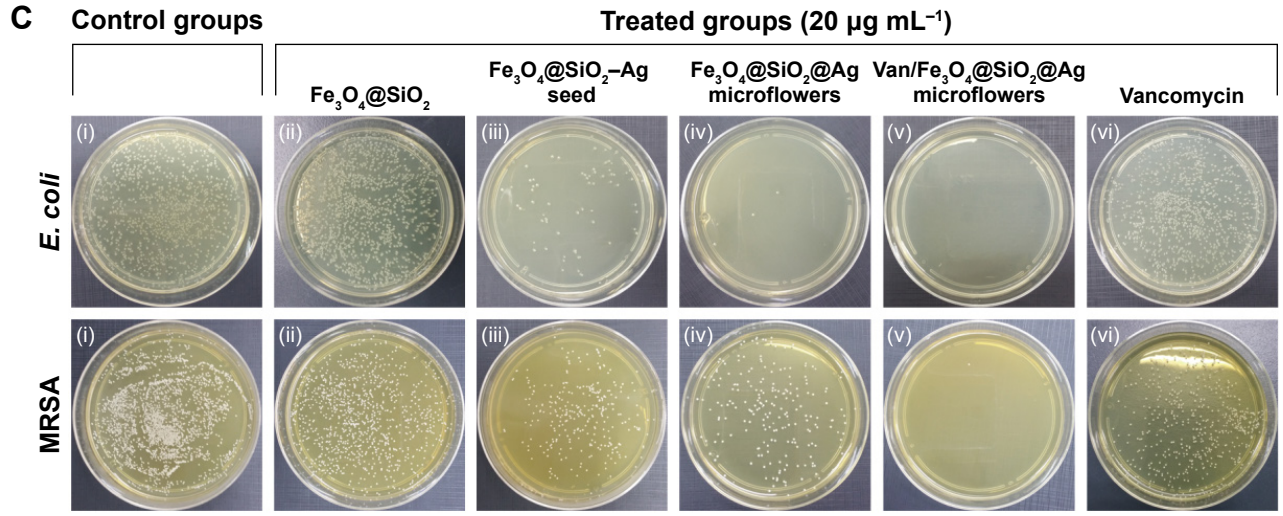

Figure 4 (**A** and **B**) Bacterial growth curves in culture media with Van/Fe_3O_4@SiO_2@Ag microflowers. Different concentrations of vancomycin-modified Ag microflowers were used in the cultures of (**A**) *Escherichia coli* and (**B**) methicillin-resistant *Staphylococcus aureus* (MRSA). The growth of the bacteria was measured by determination of optical density (OD) at wavelength of 600 nm. (**C**) Photographs showing viability of *E. coli* and MRSA after treatment under different synthesized products at a concentration of 20 μg mL^{-1}: (i) control group, (ii) Fe_3O_4@SiO_2, (iii) Fe_3O_4@SiO_2–Ag seed, (iv) Fe_3O_4@SiO_2@Ag microflowers, (v) Van/Fe_3O_4@SiO_2@Ag microflowers, and (vi) free-form vancomycin.

of bacterial colonies in the control and treated groups of different microstructures after 12-h cultivation. The control (absence of particles) and Fe_3O_4@SiO_2 microsphere-treated solutions did not inhibit the bacterial growth. The Fe_3O_4@SiO_2–Ag seed showed higher antibacterial efficiency compared with its precursor Fe_3O_4@SiO_2 microspheres. After the decoration of Ag seeds and flower-like Ag petals, the number of *E. coli* and MRSA colonies gradually decreased. These results prove that Ag-coated magnetic microcomposites exhibit antibacterial activities against both Gram-negative and Gram-positive bacterial pathogens. The bactericidal effect also increased significantly with increasing Ag coating components surrounding the magnetic core. Few colonies of *E. coli* were found during treatment with the Fe_3O_4@SiO_2@Ag microflowers, whereas bacterial colonies of MRSA were still observed in Ag microflower-treated group. MRSA showed less susceptibility to the Fe_3O_4@SiO_2@Ag microflowers than *E. coli*. The Fe_3O_4@SiO_2@Ag microflowers cannot effectively kill MRSA at 20 μg mL^{-1} within 60 min. However, almost no colonies of both Gram-negative (*E. coli*) and Gram-positive (MRSA) bacterial strains were observed during treatment with the Van/Fe_3O_4@SiO_2@Ag microflowers, indicating the inactivation of most bacteria. Picture (vi) of Figure 4C shows the photograph taken from the vancomycin-treated bacteria sample that was incubated for 1 h. The colony number was slightly smaller than that observed in the control groups, indicating that vancomycin molecules are not effective at 20 μg mL^{-1} in such a short time. Hence, the activity of the fabricated Van/Fe_3O_4@SiO_2@Ag microflowers against bacteria, especially MRSA, was enhanced when combined with vancomycin. These results indicate the presence of synergistic effect between the microflowers and vancomycin.

Fluorescence-based cell viability assay was performed to determine the bacterial survival rate and demonstrate the relation between the bactericidal effect and the sterilization duration at a fixed concentration of Van/Fe_3O_4@SiO_2@Ag microflowers (20 μg mL^{-1}). The live/dead staining technique contains two nucleic dyes, SYTO9 and propidium iodide (PI), to quantify live and dead microbes from the fluorescence microscopy images.[11] The SYTO9 can enter bacterial cell membrane and label DNA to produce green color for living bacteria, while PI only binds to the nucleic acid of the dead cells with destroyed membrane and shows red fluorescence. As shown in Figure 5A, the number of live bacteria decreased with prolonged sterilization. Almost no red fluorescence can be observed at the beginning of the test, which indicated that most bacteria are alive. After the bacteria were incubated with the Van/Fe_3O_4@SiO_2@Ag microflower solution for different durations, almost all *E. coli* colonies were killed in less than 45 min, whereas 99% of MRSA colonies were killed within 60 min. Thus, the bactericidal activity of Van/Fe_3O_4@SiO_2@Ag microflowers depends on the concentration of the microflowers and the incubation time. The representative time-dependent bacterial viability rates are shown in Figure 5B. We finally examined the morphological changes

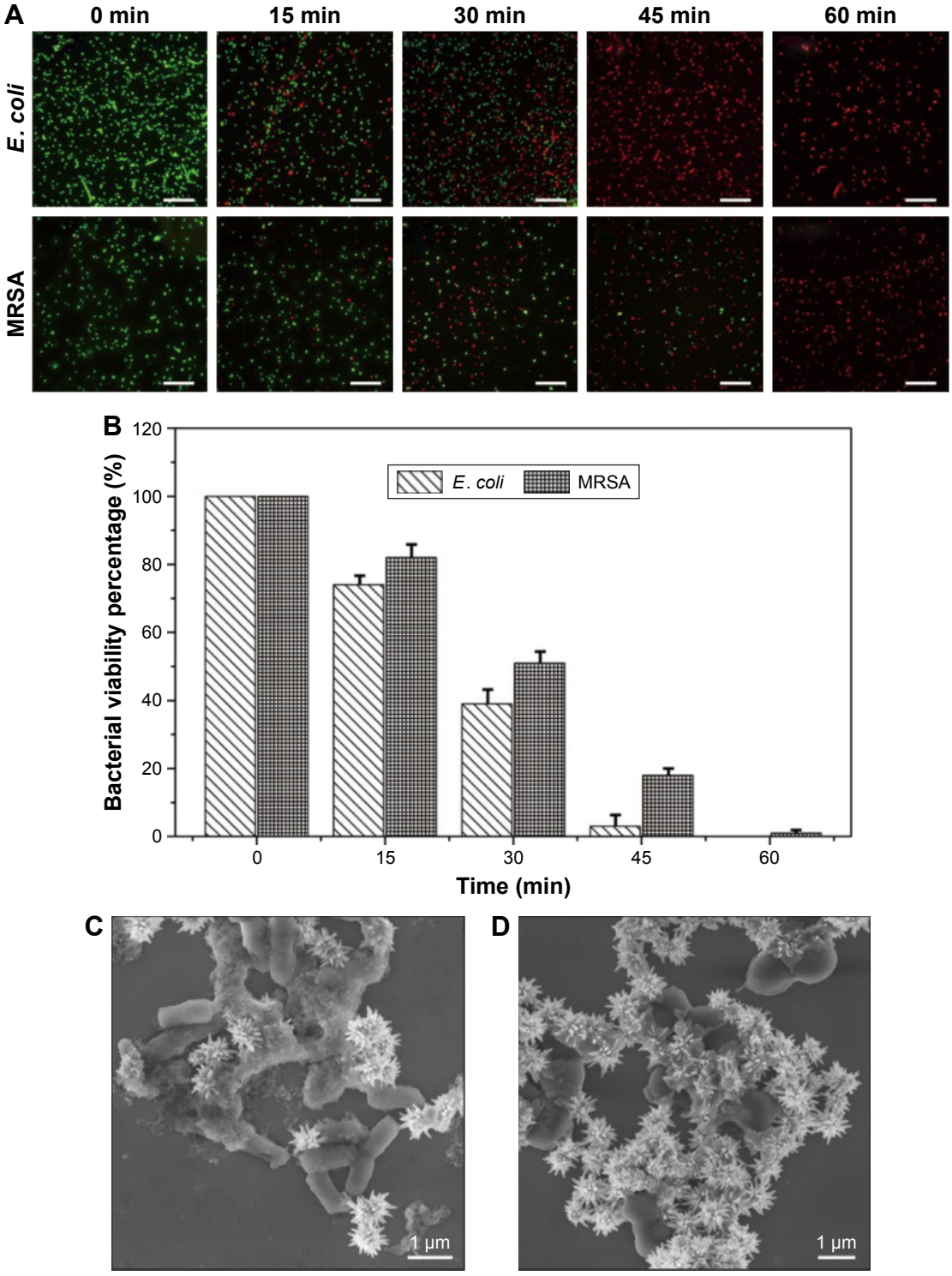

Figure 5 (**A**) Fluorescence microscopy images of live and dead *Escherichia coli* and methicillin-resistant *Staphylococcus aureus* (MRSA) treated with 20 μg mL^{-1} Van/Fe_3O_4@SiO_2@Ag microflowers for different durations. The red color indicates dead bacteria, and the green color denotes live bacterial cells. Scale bar is 20 μm. (**B**) Percentage survival of bacterial cells (counted with live/dead bacterial kit). Data are expressed as mean ± standard deviation (n=3). (**C** and **D**) Scanning electron microscopy images of *E. coli* and MRSA after 60 min of incubation with Van/Fe_3O_4@SiO_2@Ag microflowers.

in the bacterial cells after the antimicrobial treatment. Figure 5C and D shows the SEM micrographs of *E. coli* and MRSA after incubation with Van/Fe_3O_4@SiO_2@Ag microflowers for 60 min, respectively. Treated rod-like *E. coli* cells (Figure 5C) showed extensive membrane damage and leaked intracellular components, resulting in shrinkage and lysis of cells. Similarly, extensive membrane lysis and significant reduction in the size of the treated grape-like

MRSA cells were observed (Figure 5D). The significant bacterial cell damage and changes in the cell morphology within such a short time could be mainly due to the interactions of Van/Fe_3O_4@SiO_2@Ag microflowers with the cell wall; this interaction enhanced permeability of the membrane and accelerated bacterial cell disruption. These results further demonstrate the rapid and efficient sterilization capacity of the synthesized Van/Fe_3O_4@SiO_2@Ag microflowers.

Recyclability of Van/Fe_3O_4@SiO_2@Ag microflowers

Recyclability is the main advantage of the fabricated Van/Fe_3O_4@SiO_2@Ag microflowers over other traditional antibacterial nanomaterials. The magnetic property renders the Van/Fe_3O_4@SiO_2@Ag microflowers to be facilely controlled by an external magnetic force after bactericidal behavior and makes the recovered microcomposites ready for a new antimicrobial cycle (Scheme 1B). Recyclability tests were performed with *E. coli* (10 μg mL^{-1}) and MRSA (20 μg mL^{-1}) using plate counting method; after five magnetic separation cycles, the antimicrobial effect was maintained at ~95% and 90%, respectively. This result suggests that the recycled Van/Fe_3O_4@SiO_2@Ag microflowers remained stable and exhibited excellent sterilization abilities (Figure 6). The decrease in the antimicrobial effect may be due to leakage of Ag during incubation in bacterial solution or covering of the active vancomycin-modified Ag surface by interferents, such as peptidoglycan, proteins, and nucleic acids, released from the killed bacterial cells. The chemical structure of the Van/Fe_3O_4@SiO_2@Ag microflowers was checked after the recycling by TGA and DSC analysis. No big differences were found between the materials before and after recycling which indicated that the chemical structure was maintained after five antimicrobial cycles (Figure S6). The potential recyclability of the magnetic microflowers provides a novel and green approach toward eliminating the one-time-use problem of traditional antibacterial materials.

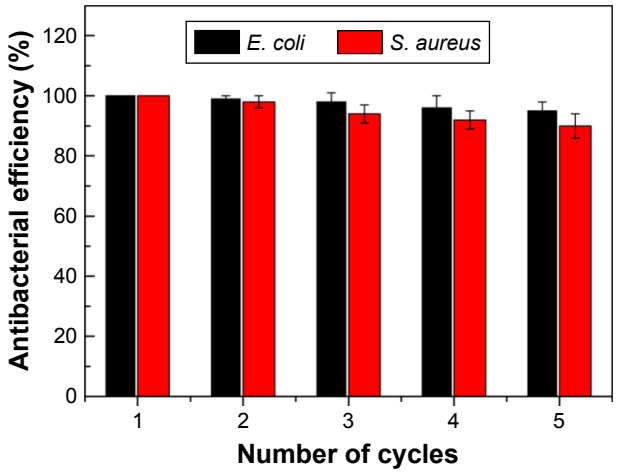

Figure 6 Antibacterial effect of recycled Van/Fe_3O_4@SiO_2@Ag microflowers against *Escherichia coli* (10 μg mL^{-1}) and methicillin-resistant *Staphylococcus aureus* (20 μg mL^{-1}). The error bars represent the standard deviation of the experiments performed in triplicate.

Antibacterial mechanism of Van/Fe_3O_4@SiO_2@Ag microflowers

Overall, the results of real-time bacterial growth monitoring, agar plate colony analysis, and live/dead cell staining observations indicate the enhanced antibacterial efficiency of the fabricated Van/Fe_3O_4@SiO_2@Ag microflowers against both Gram-negative (*E. coli*) and Gram-positive (MRSA) bacteria as well as the poor bactericidal effect of the same concentration of Fe_3O_4@SiO_2@Ag microflowers against MRSA. The mechanism underlying the synergistic effect of the Ag microflower and vancomycin must be further clarified. Studies showed that the antimicrobial properties of Ag materials rely on free Ag ions, which can not only bind to sulfur, oxygen, and nitrogen of essential enzymes, resulting in bacterial cell death, but also react with DNA to prevent unwinding, resulting in serious damage to bacterial cells.[29,50,51] Moreover, the Ag NPs itself can directly deactivate the sulfur-containing proteins of cell membrane, causing functional damage to the membrane and the structural changes.[52]

On the other hand, vancomycin is a potent antibiotic against Gram-positive bacteria and exerts antibacterial activity by forming hydrogen bonds with the peptidoglycan terminus D-Ala-D-Ala on the cell wall. This phenomenon inhibits the synthesis of the bacterial cell wall. Moreover, Gram-negative bacteria can be captured by vancomycin because of either unspecific binding between receptors on the pathogen surface and the glycosides on the vancomycin moiety or deformities/breaks in the outer membrane of Gram-negative bacteria, exposing the D-Ala-D-Ala groups on the interior bacterial surface.[37] Therefore, vancomycin-modified nanostructures can interact strongly with a broad range of Gram-positive and Gram-negative bacteria and thus can be used as affinity probes to selectively trap these organisms.[21,53]

On the basis of the knowledge in the previous studies combined with our experimental results, the plausible mechanism of the enhanced antibacterial activity of Van/Fe_3O_4@SiO_2@Ag microflowers is proposed in Figure 7A. The Van/Fe_3O_4@SiO_2@Ag microflower can interact with the cell wall of the bacteria and adhere onto the bacterial surface

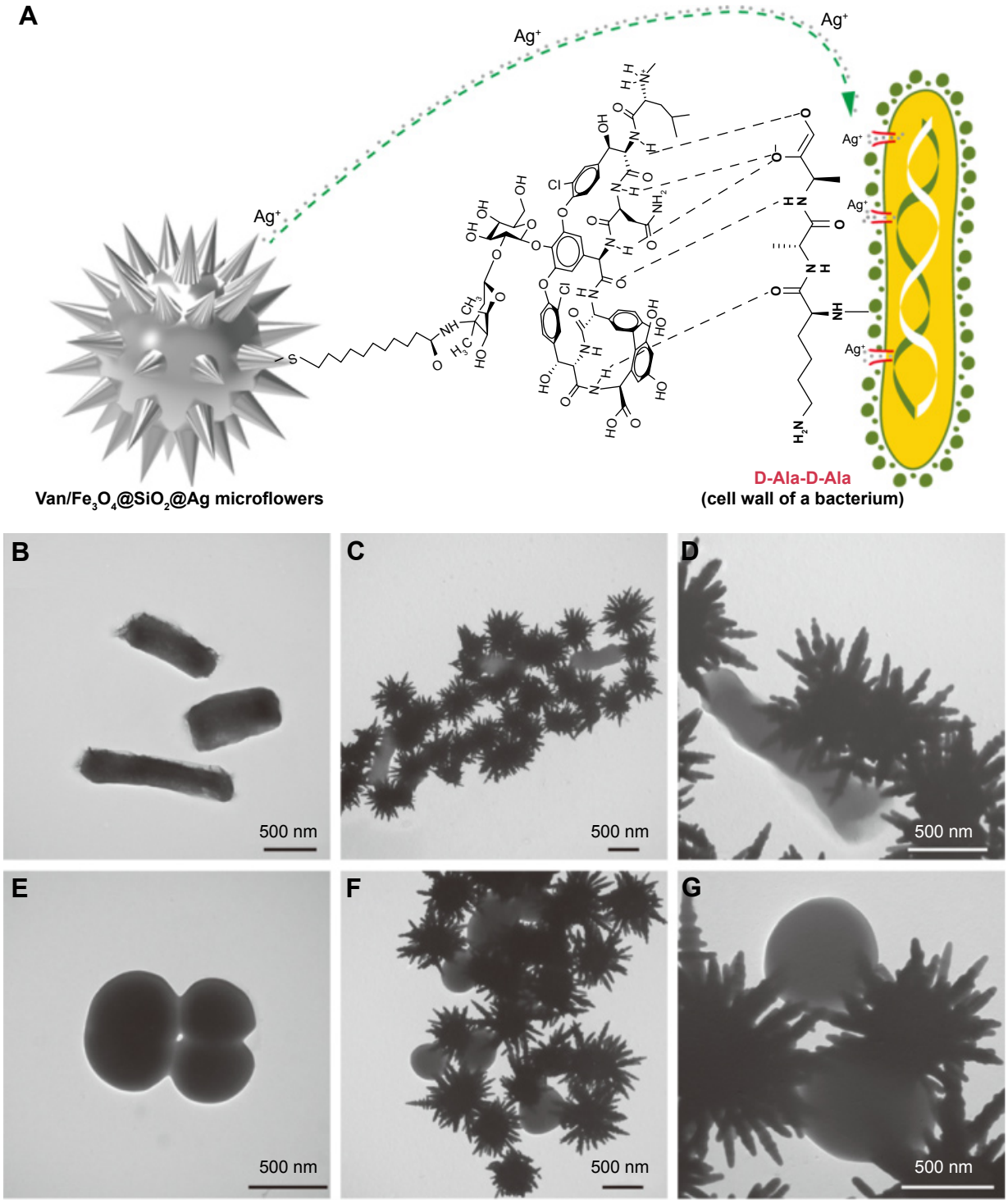

Figure 7 (**A**) Mechanism of the synergistic antibacterial effect of vancomycin with Fe_3O_4@SiO_2@Ag microflowers. Transmission electron microscopy images of (**B**) *Escherichia coli* (control) and (**C** and **D**) *E. coli* treated with Van/Fe_3O_4@SiO_2@Ag microflowers, and (**E**) methicillin-resistant *Staphylococcus aureus* (MRSA) (control) and (**F** and **G**) MRSA treated with Van/Fe_3O_4@SiO_2@Ag microflowers. (**D** and **G**) Increased magnifications of (**C**) and (**F**), respectively.

through its surface-modified vancomycin layer. Through direct contact, the vancomycin layer plays important roles in destroying the structure of the cell wall and increasing the permeability of the cell membrane. Moreover, the highly branched petals of the Ag microflowers act as extended arms in highly active surface areas for bacterial contact and Ag ion release. This phenomenon leads to rapid cell wall lysis and enhanced penetration of the Ag ions into the bacterium. The TEM studies clearly show that the Van/Fe_3O_4@SiO_2@Ag microflowers can effectively bind to both *E. coli* and

MRSA, and the Ag petals of the microflowers are closely attached to the cell wall (Figure 7B–G). We believe that vancomycin-modified Ag petals interact with the cell membrane and adhere onto the bacterial surface, leading to disorganized permeability of the cell membrane, speeding up Ag ions entry into bacterium, and eventually causing cell death.

Conclusion

A newly developed Van/Fe_3O_4@SiO_2@Ag microflower with enhanced antibacterial activity is experimentally and theoretically presented in this study. The obtained microcomposite comprised three parts: a submicron-scale magnetic core to provide sufficient magnetic response property, a flower-like Ag shell to build highly active areas for Ag ion release and bacterial contact, and an ultrathin vancomycin layer to bind to the bacterial cell wall and increase the cell membrane permeability. The detailed nanostructures of the products were characterized by HRTEM, SEM, EDX, XRD, and elemental mapping analyses. The Van/Fe_3O_4@SiO_2@Ag microflowers can rapidly and effectively kill both *E. coli* and MRSA at low concentrations. The killing efficiency can be increased to a high level. The MIC of the enhanced effect of the Van/Fe_3O_4@SiO_2@Ag microflowers decreased by ~60% for *E. coli* and 63.5% for MRSA compared with that using only Fe_3O_4@SiO_2@Ag microflowers. Thus, we think the effectiveness of vancomycin-modified Fe_3O_4@SiO_2@Ag microflowers against resistant strains such as MRSA provides a very simple but highly efficient strategy to combat drug-resistant bacterial infections. Moreover, the magnetic property renders the Van/Fe_3O_4@SiO_2@Ag microflowers to be facilely controlled by an orientation magnetic field after antibacterial behavior. The recovered products can then be reused many times. We further demonstrated that the antimicrobial effect of the fabricated Van/Fe_3O_4@SiO_2@Ag microflower was maintained at no less than 90% after cycling for five times, indicating the high stability of the product. Hence, the Van/Fe_3O_4@SiO_2@Ag microflowers are potential effective and recyclable antibacterial agent for medical and environmental applications.

Acknowledgments

This work was supported by grants from the National Natural Science Foundation of China (No 81230089), National High Technology Research and Development Program of China (No 2015AA020929), Beijing Municipal Science & Technology Commission (No Z161100000116040), and Beijing Nova Program (No Z141107001814071).

Disclosure

The authors report no conflicts of interest in this work.

References

1. Wang Y, Ding X, Chen Y, et al. Antibiotic-loaded, silver core-embedded mesoporous silica nanovehicles as a synergistic antibacterial agent for the treatment of drug-resistant infections. *Biomaterials*. 2016;101:207–216.
2. Neu HC. The crisis in antibiotic resistance. *Science*. 1992;257(5073):1064–1073.
3. Hussein-Al-Ali SH, El Zowalaty ME, Hussein MZ, Ismail M, Webster TJ. Synthesis, characterization, controlled release, and antibacterial studies of a novel streptomycin chitosan magnetic nanoantibiotic. *Int J Nanomedicine*. 2014;9:549–557.
4. Huang CJ, Chen YS, Chang Y. Counterion-activated nanoactuator: reversibly switchable killing/releasing bacteria on polycation brushes. *ACS Appl Mater Interfaces*. 2015;7(4):2415–2423.
5. Chudasama B, Vala AK, Andhariya N, Upadhyay RV, Mehta RV. Enhanced antibacterial activity of bifunctional Fe_3O_4-Ag core-shell nanostructures. *Nano Res*. 2009;2(12):955–965.
6. Regiel-Futyra A, Kus-Liśkiewicz M, Sebastian V, et al. Development of noncytotoxic chitosan-gold nanocomposites as efficient antibacterial materials. *ACS Appl Mater Interfaces*. 2015;7(2):1087–1099.
7. Lv M, Su S, He Y, et al. Long-term antimicrobial effect of silicon nanowires decorated with silver nanoparticles. *Adv Mater*. 2010;22(48):5463–5467.
8. Kim YH, Lee DK, Cha HG, Kim CW, Kang YC, Kang YS. Preparation and characterization of the antibacterial Cu nanoparticle formed on the surface of SiO_2 nanoparticles. *J Phys Chem B*. 2006;110(49):24923–24928.
9. Agnihotri S, Bajaj G, Mukherji S, Mukherji S. Arginine-assisted immobilization of silver nanoparticles on ZnO nanorods: an enhanced and reusable antibacterial substrate without human cell cytotoxicity. *Nanoscale*. 2015;7(16):7415–7429.
10. Hu W, Peng C, Luo W, et al. Graphene-based antibacterial paper. *ACS Nano*. 2010;4(7):4317–4323.
11. Quirós J, Borges JP, Boltes K, Rodea-Palomares I, Rosal R. Antimicrobial electrospun silver-, copper- and zinc-doped polyvinylpyrrolidone nanofibers. *J Hazard Mater*. 2015;299:298–305.
12. Tan P, Li YH, Liu XQ, Jiang Y, Sun LB. Core–shell AgCl@SiO_2 nanoparticles: Ag(I)-based antibacterial materials with enhanced stability. *ACS Sustainable Chem Eng*. 2016;4(6):3268–3275.
13. Maleki A, Movahed H, Paydar R. Design and development of a novel cellulose/γ-Fe_2O_3/Ag nanocomposite: a potential green catalyst and antibacterial agent. *RSC Adv*. 2016;6(17):13657–13665.
14. Shome A, Dutta S, Maiti S, Das PK. In situ synthesized Ag nanoparticle in self-assemblies of amino acid based amphiphilic hydrogelators: development of antibacterial soft nanocomposites. *Soft Matter*. 2011;7(6):3011–3022.
15. Sureshkumar M, Siswanto DY, Lee CK. Magnetic antimicrobial nanocomposite based on bacterial cellulose and silver nanoparticles. *J Mater Chem*. 2010;20(33):6948–6955.
16. Liu H, Lv M, Deng B, et al. Laundering durable antibacterial cotton fabrics grafted with pomegranate-shaped polymer wrapped in silver nanoparticle aggregations. *Sci Rep*. 2014;4:5920.
17. Prucek R, Tuček J, Kilianová M, et al. The targeted antibacterial and antifungal properties of magnetic nanocomposite of iron oxide and silver nanoparticles. *Biomaterials*. 2011;32(21):4704–4713.
18. Zhang X, Niu H, Yan J, Cai Y. Immobilizing silver nanoparticles onto the surface of magnetic silica composite to prepare magnetic disinfectant with enhanced stability and antibacterial activity. *Colloids Surf A Physicochem Eng Asp*. 2011;375(1–3):186–192.
19. Cong Y, Xia T, Zou M, et al. Mussel-inspired polydopamine coating as a versatile platform for synthesizing polystyrene/Ag nanocomposite particles with enhanced antibacterial activities. *J Mater Chem B*. 2014;2(22):3450–3461.

20. Liu L, Yang J, Xie J, et al. The potent antimicrobial properties of cell penetrating peptide-conjugated silver nanoparticles with excellent selectivity for gram-positive bacteria over erythrocytes. *Nanoscale*. 2013;5(9):3834–3840.
21. Ray PC, Khan SA, Singh AK, Senapati D, Fan Z. Nanomaterials for targeted detection and photothermal killing of bacteria. *Chem Soc Rev*. 2012;41(8):3193–3209.
22. Jeong CJ, Sharker SM, In I, Park SY. Iron oxide@PEDOT-based recyclable photothermal nanoparticles with poly(vinylpyrrolidone) sulfobetaines for rapid and effective antibacterial activity. *ACS Appl Mater Interfaces*. 2015;7(18):9469–9478.
23. Xiong R, Lu C, Wang Y, Zhou Z, Zhang X. Nanofibrillated cellulose as the support and reductant for the facile synthesis of Fe_3O_4/Ag nanocomposites with catalytic and antibacterial activity. *J Mater Chem A*. 2013;1(47):14910–14918.
24. Chen SS, Xu H, Xu HJ, et al. A facile ultrasonication assisted method for Fe_3O_4@SiO_2-Ag nanospheres with excellent antibacterial activity. *Dalton Trans*. 2015;44(19):9140–9148.
25. Singh MP, Raghupathy Y, Natarajan KA, Srivastava C. Synthesis, electron microscopy and anti-microbial properties of Fe_3O_4–Ag nanotubes. *RSC Adv*. 2015;5(48):38164–38169.
26. Lin L, Cui H, Zeng G, et al. Ag–$CuFe_2O_4$ magnetic hollow fibers for recyclable antibacterial materials. *J Mater Chem B*. 2013;1(21):2719–2723.
27. Kooti M, Gharineh S, Mehrkhah M, Shaker A, Motamedi H. Preparation and antibacterial activity of $CoFe_2O_4$/SiO_2/Ag composite impregnated with streptomycin. *Chem Eng J*. 2015;259:34–42.
28. Panáček A, Smékalová M, Večeřová R, et al. Silver nanoparticles strongly enhance and restore bactericidal activity of inactive antibiotics against multiresistant enterobacteriaceae. *Colloids Surf B Biointerfaces*. 2016;142:392–399.
29. Deng H, McShan D, Zhang Y, et al. Mechanistic study of the synergistic antibacterial activity of combined silver nanoparticles and common antibiotics. *Environ Sci Technol*. 2016;50(16):8840–8848.
30. Wan Y, Zhang D, Wang Y, Qi P, Wu J, Hou B. Vancomycin-functionalised Ag@TiO_2 phototoxicity for bacteria. *J Hazard Mater*. 2011;186(1):306–312.
31. Brown AN, Smith K, Samuels TA, Lu J, Obare SO, Scott ME. Nanoparticles functionalized with ampicillin destroy multiple-antibiotic-resistant isolates of Pseudomonas aeruginosa and Enterobacter aerogenes and methicillin-resistant Staphylococcus aureus. *Appl Environ Microbiol*. 2012;78(8):2768–2774.
32. Lai HZ, Chen WY, Wu CY, Chen YC. Potent antibacterial nanoparticles for pathogenic bacteria. *ACS Appl Mater Interfaces*. 2015;7(3):2046–2054.
33. Wang C, Wang J, Li P, et al. Sonochemical synthesis of highly branched flower-like Fe_3O_4@SiO_2@Ag microcomposites and their application as versatile SERS substrates. *Nanoscale*. 2016;8(47):19816–19828.
34. Esmaeili A, Ghobadianpour S. Vancomycin loaded superparamagnetic $MnFe_2O_4$ nanoparticles coated with PEGylated chitosan to enhance antibacterial activity. *Int J Pharm*. 2016;501(1–2):326–330.
35. Gu H, Ho PL, Tong E, Wang L, Xu B. Presenting vancomycin on nanoparticles to enhance antimicrobial activities. *Nano Lett*. 2003;3(9):1261–1263.
36. Lai BH, Chen DH. Vancomycin-modified LaB6@SiO_2/Fe_3O_4 composite nanoparticles for near-infrared photothermal ablation of bacteria. *Acta Biomater*. 2013;9(7):7573–7579.
37. Kell AJ, Stewart G, Ryan S, et al. Vancomycin-modified nanoparticles for efficient targeting and preconcentration of gram-positive and gram-negative bacteria. *ACS Nano*. 2008;2(9):1777–1788.
38. Xuan S, Wang F, Wang YJ, Yu JC, Leung KC. Facile synthesis of size-controllable monodispersed ferrite nanospheres. *J Mater Chem*. 2010;20(24):5086–5094.
39. Wang J, Wu X, Wang C, et al. Magnetically assisted surface-enhanced Raman spectroscopy for the detection of Staphylococcus aureus based on aptamer recognition. *ACS Appl Mater Interfaces*. 2015;7(37):20919–20929.
40. Wang Y, Wang K, Zou B, et al. Magnetic-based silver composite microspheres with nanosheet-assembled shell for effective SERS substrate. *J Mater Chem C*. 2013;1(13):2441–2447.
41. Kim K, Lee YM, Lee HB, Shin KS. Silver-coated silica beads applicable as core materials of dual-tagging sensors operating via SERS and MEF. *ACS Appl Mater Interfaces*. 2009;1(10):2174–2180.
42. Rong Z, Xiao R, Wang C, Wang D, Wang S. Plasmonic Ag core-satellite nanostructures with a tunable silica-spaced nanogap for surface-enhanced Raman scattering. *Langmuir*. 2015;31(29):8129–8137.
43. Wang C, Xu J, Wang J, et al. Polyethylenimine-interlayered silver-shell magnetic-core microspheres as multifunctional SERS substrates. *J Mater Chem C*. 2015;3(33):8684–8693.
44. Wang C, Wang J, Li M, et al. A rapid SERS method for label-free bacteria detection using polyethylenimine-modified Au-coated magnetic microspheres and Au@Ag nanoparticles. *Analyst*. 2016;141(22):6226–6238.
45. Zhang M, Zhao A, Wang D, Sun H. Hierarchically assembled NiCo@SiO_2@Ag magnetic core-shell microspheres as highly efficient and recyclable 3D SERS substrates. *Analyst*. 2015;140(2):440–448.
46. Wang C, Li P, Wang J, et al. Polyethylenimine-interlayered core-shell-satellite 3D magnetic microspheres as versatile SERS substrates. *Nanoscale*. 2015;7(44):18694–18707.
47. An Q, Zhang P, Li JM, et al. Silver-coated magnetite-carbon core-shell microspheres as substrate-enhanced SERS probes for detection of trace persistent organic pollutants. *Nanoscale*. 2012;4(16):5210–5216.
48. Wang J, Wu X, Wang C, et al. Facile synthesis of Au-coated magnetic nanoparticles and their application in bacteria detection via a SERS method. *ACS Appl Mater Interfaces*. 2016;8(31):19958–19967.
49. Zhu M, Liu W, Liu H, et al. Construction of Fe_3O_4/vancomycin/PEG magnetic nanocarrier for highly efficient pathogen enrichment and gene sensing. *ACS Appl Mater Interfaces*. 2015;7(23):12873–12881.
50. Hajipour MJ, Fromm KM, Ashkarran AA, et al. Antibacterial properties of nanoparticles. *Trends Biotechnol*. 2012;30(10):499–511.
51. Fayaz AM, Balaji K, Girilal M, Yadav R, Kalaichelvan PT, Venketesan R. Biogenic synthesis of silver nanoparticles and their synergistic effect with antibiotics: a study against gram-positive and gram-negative bacteria. *Nanomedicine*. 2010;6(1):103–109.
52. Xu WP, Zhang LC, Li JP, et al. Facile synthesis of silver@graphene oxide nanocomposites and their enhanced antibacterial properties. *J Mater Chem*. 2011;21(12):4593–4597.
53. Liu TY, Tsai KT, Wang HH, et al. Functionalized arrays of Raman-enhancing nanoparticles for capture and culture-free analysis of bacteria in human blood. *Nat Commun*. 2011;2:538.

Supplementary materials

Results	Mean (mV)	Area (%)	Width (mV)
Zeta potential (mV): –31.3	Peak 1: –31.3	100.0	8.57
Zeta deviation (mV): 8.57	Peak 2: 0.00	0.0	0.00
Conductivity (mS/cm): 0.0176	Peak 3: 0.00	0.0	0.00
Result quality Good			

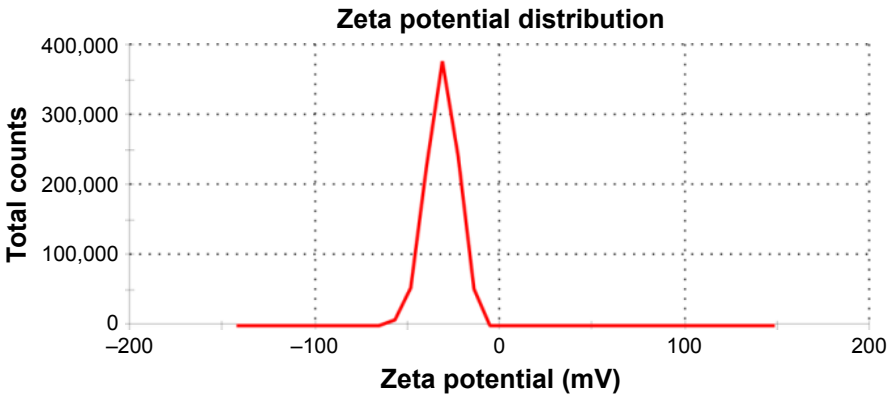

Figure S1 Zeta potential of Fe_3O_4@SiO_2 microspheres in ethanol.

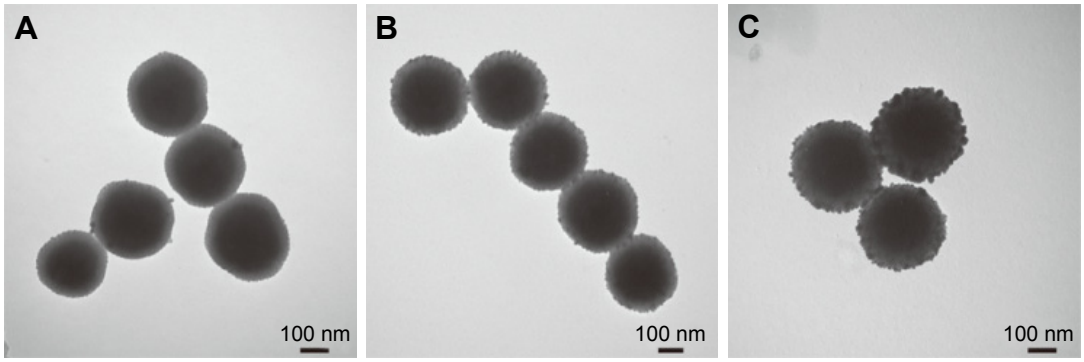

Figure S2 Transmission electron microscopy images of Fe_3O_4@SiO_2–Ag seed synthesized with different concentrations of $AgNO_3$: (**A**) 0.2, (**B**) 0.4, and (**C**) 0.8 mM.

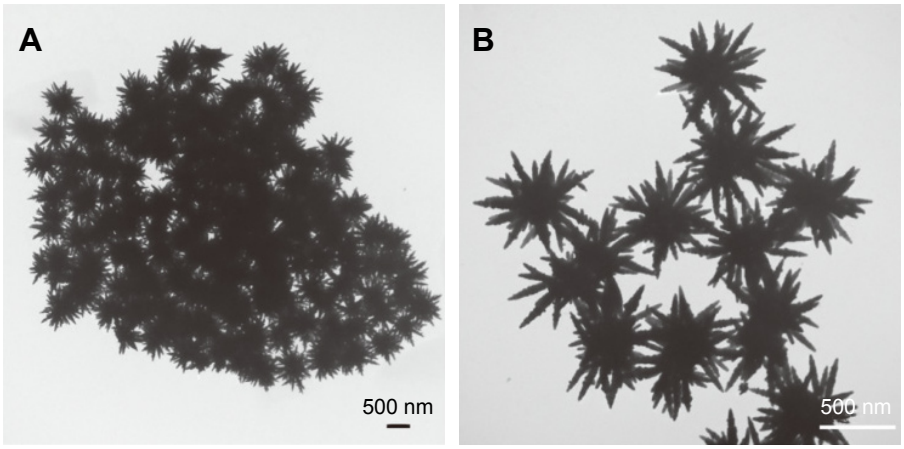

Figure S3 Transmission electron microscopy images of Fe_3O_4@SiO_2@Ag microflowers synthesized (**A**) without polyvinylpyrrolidone (PVP) and (**B**) with 1 mg/mL PVP.

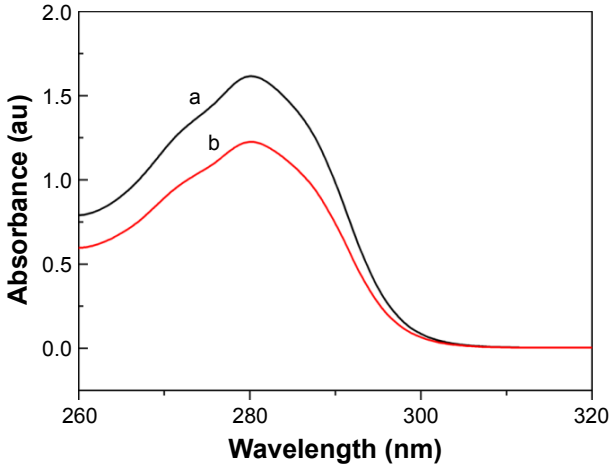

Figure S4 Absorption spectra of vancomycin solution (a) before and (b) after binding to 11-mercaptoundecanoic acid-modified Fe_3O_4@SiO_2@Ag microflowers.

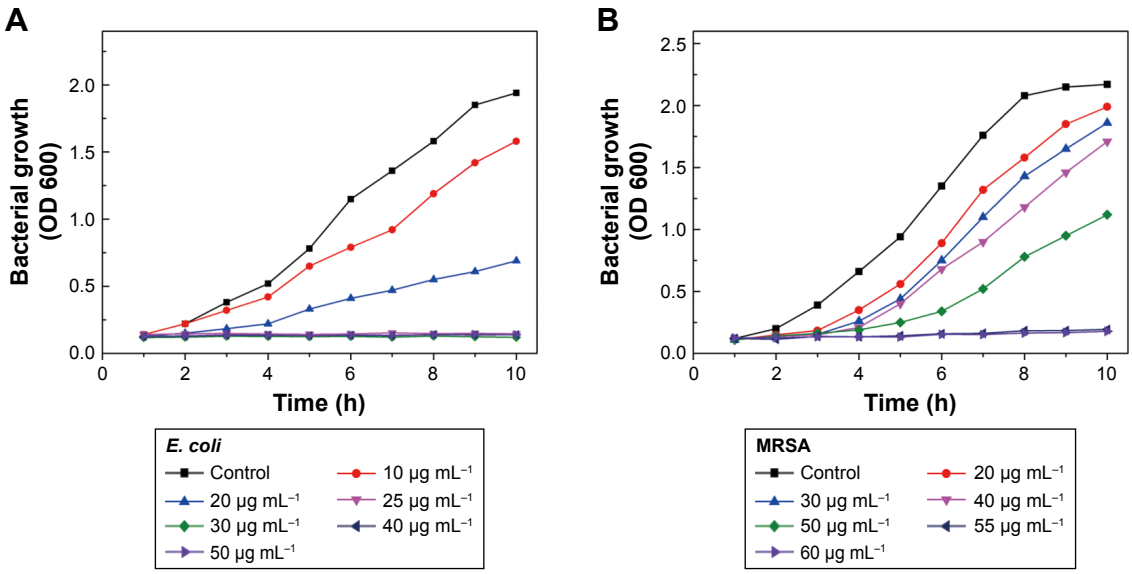

Figure S5 Bacterial growth curves are employed to evaluate the antibacterial activities of the Fe_3O_4@SiO_2@Ag microflowers against (**A**) *Escherichia coli* and (**B**) methicillin-resistant *Staphylococcus aureus* (MRSA). Different concentrations of the Fe_3O_4@SiO_2@Ag microflowers were added to the culture of *E. coli* and MRSA (10–50 and 20–60 μg mL^{-1}, respectively). The control group was tested in the absence of Fe_3O_4@SiO_2@Ag microflowers. The growth of bacteria was assessed by determining optical density (OD) at a wavelength of 600 nm.

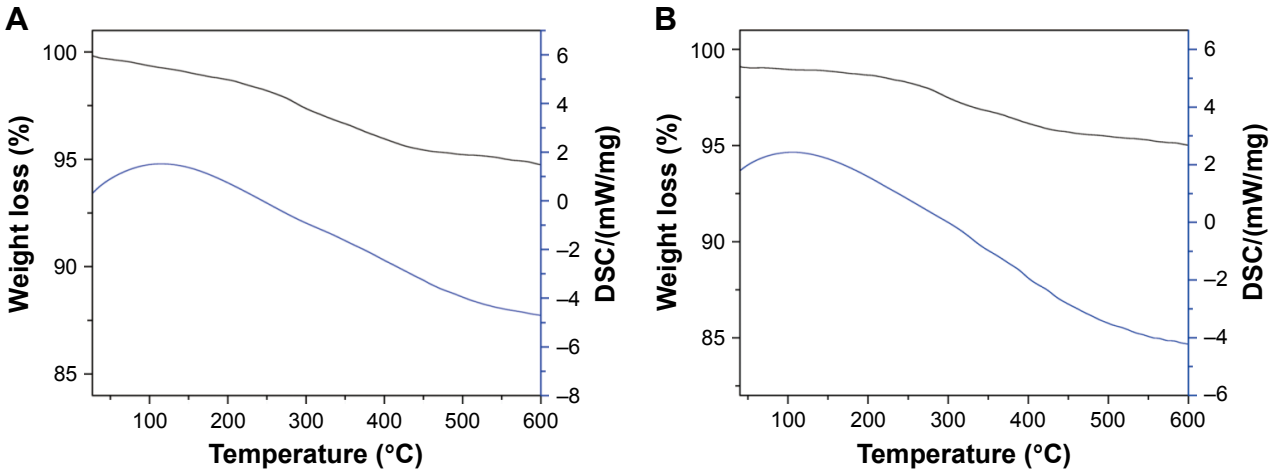

Figure S6 Thermogravimetric analysis (blank line) and differential scanning calorimetry (DSC) (blue line) curves of Van/Fe_3O_4@SiO_2@Ag microflowers (**A**) before and (**B**) after five antimicrobial cycles.